Research Paper

THEMED ISSUE: Subduction Top to Bottom 2

GEOSPHERE

GEOSPHERE

https://doi.org/10.1130/GES02473.1

8 figures; 1 supplemental file

CORRESPONDENCE: geb0@lehigh.edu

CITATION: Bebout, G.E., Ota, T., Kunihiro, T., Carlson, W.D., and Nakamura, E., 2022, Lithium in garnet as a tracer of subduction zone metamorphic reactions: The record in ultrahigh-pressure metapelites at Lago di Cignana, Italy: Geosphere, https://doi.org/10.1130/GES02473.1.

Science Editor: Shanaka de Silva
Guest Associate Editor: David W. Scholl

Received 27 July 2021
Revision received 17 December 2021
Accepted 28 February 2022

Published online 22 April 2022

Lithium in garnet as a tracer of subduction zone metamorphic reactions: The record in ultrahigh-pressure metapelites at Lago di Cignana, Italy

Gray E. Bebout[1,2], Tsutomu Ota[1], Takuya Kunihiro[1], William D. Carlson[3,*], and Eizo Nakamura[1]

[1]Pheasant Memorial Laboratory for Geochemistry and Cosmochemistry, Institute for Planetary Materials, Okayama University, Misasa, Tottori, 682-0193, Japan
[2]Department of Earth and Environmental Sciences, Lehigh University, Bethlehem, Pennsylvania 18015, USA
[3]Department of Geological Sciences, Jackson School of Geosciences, University of Texas at Austin, Austin, Texas 78712, USA

ABSTRACT

Lithium is of great interest as a tracer of metamorphic reactions and related fluid-mineral interactions because of its potential to isotopically fractionate during inter- and intracrystalline diffusional processes. Study of its transfer through subduction zones, based on study of arc volcanic and metamorphic rocks, can yield insight regarding ocean-to-mantle chemical cycling.

We investigated major- and trace-element concentrations and δ^7Li in garnet in ultrahigh-pressure (UHP) Lago di Cignana metasedimentary rocks, relating these observations to reconstructed prograde devolatilization history. In all garnet crystals we studied, heavy rare earth elements (HREEs), Y, and Li showed strong zoning, with elevated concentrations in cores (15–50 ppm Li) and marked high-concentration anomalies (up to 117 ppm Li, 5500 ppm Y; little or no major-element shift) as growth annuli, in which some crystals showed subtle elevation in δ^7Li greater than analytical error of ~3‰ (2σ). Rutile inclusions appeared abruptly at annuli and outward toward rims, accompanied by inclusions of a highly zoned, Ca- and rare earth element–rich phase and decreased Nb concentrations in garnet. These relationships are interpreted to reflect prograde garnet-forming reaction(s), in part involving titanite breakdown to stabilize rutile, which resulted in delivery of more abundant Y and HREEs at surfaces of growing garnet crystals to produce annuli. Co-enrichments in Li and Y + REEs are attributed to mutual incorporation via charge-coupled substitutions; thus, increased Li uptake was a passive consequence of elevated concentrations of Y + REEs. The small-scale fluctuations in δ^7Li (overall range of ~9‰) observed in some crystals may correlate with abrupt shifts in major- and trace-element concentrations, suggesting that changes in reactant phases exerted some control on the evolution of δ^7Li. For one garnet crystal, late-stage growth following partial resorption produced deviation in major- and trace-element compositions, including Li concentration, accompanied by a 10‰–15‰ negative shift in δ^7Li, perhaps reflecting a change in the mechanism of incorporation or source of Li.

These results highlight the value of measuring the major- and trace-element and isotope compositions of garnets in high-pressure and UHP metamorphic rocks in which matrix mineral assemblages are extensively overprinted by recrystallization during exhumation histories. Lithium concentrations and isotope compositions of the garnets can add valuable information regarding prograde (and retrograde) reaction history, kinetics of porphyroblast growth, intracrystalline diffusion, and fluid-rock interactions. This work, integrated with previous study of devolatilization in the Schistes Lustrés/Cignana metasedimentary suite, indicates retention of a large fraction of the initially subducted sedimentary Li budget to depths approaching those beneath volcanic fronts, despite the redistribution of this Li among mineral phases during complex mineral reaction histories.

Gray Bebout https://orcid.org/0000-0002-9768-9080
*Retired

INTRODUCTION

As an element that is relatively soluble in aqueous fluids and melts and that has two stable isotopes with a large relative mass difference (^{7}Li and ^{6}Li), Li offers many opportunities for addressing questions regarding fluid-rock interactions and diffusion, and related time scales (e.g., see John et al., 2012). Thus, the concentrations and isotopic compositions of Li have been measured in studies of such processes in a wide array of settings (see the review by Penniston-Dorland et al., 2017). Although a number of minerals have Li end members (e.g., spodumene, lepidolite), and tourmaline tends to be quite Li-rich (particularly elbaite), Li is generally present in silicate minerals at concentrations of up to thousands of parts per million (Bebout et al., 2013). Recently, Li concentrations have been successfully measured for whole-rock samples (by multicollector–inductively coupled plasma–mass spectrometry [MC-ICP-MS], also allowing analyses of δ^7Li; e.g., Barnes et al., 2019) and in garnets at high spatial resolution (scales of 5–15 μm) by laser-ablation (LA) ICP-MS or secondary ion mass spectrometry (SIMS) methods (e.g., Bebout et al., 2013; King et al., 2004; Cahalan et al., 2014). The existing high-resolution analyses of δ^7Li in garnet have demonstrated significant heterogeneity in some cases along gradients that appear to preserve information regarding diffusional history and related durations of diffusion (Penniston-Dorland et al., 2020; Hoover et al., 2020). In metamorphic rocks, the large relative mass difference between ^{7}Li and ^{6}Li can potentially lead to

significant fractionation during intracrystalline and intergranular diffusion (Penniston-Dorland et al., 2017, 2020; John et al., 2012).

The rates at which Li diffuses within silicate phases are related to the sites in which Li resides in those phases and the mechanisms by which the Li is incorporated. One set of detailed studies suggests that, in garnet, Li is largely incorporated as part of coupled substitutions involving Y and the heavy rare earth elements (HREEs; Carlson et al., 2014), and its intracrystalline diffusion rate is governed by the diffusion rates of these other elements (Cahalan et al., 2014). Because those elements diffuse slowly, any gradients in Li concentration and/or isotope compositions in garnet produced during growth of a crystal are likely to be preserved during later heating to relatively high temperatures. Garnet can therefore preserve detailed records of Li behavior during fluid-related and rate-dependent processes affecting its growth.

We investigated the concentrations and isotopic compositions of Li in garnet in metasedimentary rocks from the ultrahigh-pressure (UHP) metamorphic exposure at Lago di Cignana in the Italian Alps (see the map in Fig. 1). Our goals were to determine the mechanism for incorporation of Li during prograde garnet growth; to gauge whether garnet preserves records of diffusion-limited Li isotope fractionation (see the discussions by Skora et al., 2006; Moore et al., 2013); and to assess degrees of open- and closed-system behavior of the rocks during crystal growth. This work on UHP metasedimentary garnets complements that recently done by Penniston-Dorland et al. (2020) and Hoover et al. (2020) on high-pressure (HP) metabasaltic rocks in the Franciscan complex, California, and on HP metabasaltic garnets at Monviso, Italy, respectively. Our analyses of major and trace elements and Li isotope compositions of garnet are placed into the context of the detailed study of the devolatilization reaction history and fluid-rock interactions in the area (Bebout et al., 2013; Cook-Kollars et al., 2014; Epstein et al., 2020; also see Bebout and Nakamura, 2003), including investigation of whole-rock Li cycling along a high-pressure, high-temperature geotherm experienced by subduction-related rocks in the western Alps (Barnes et al., 2019).

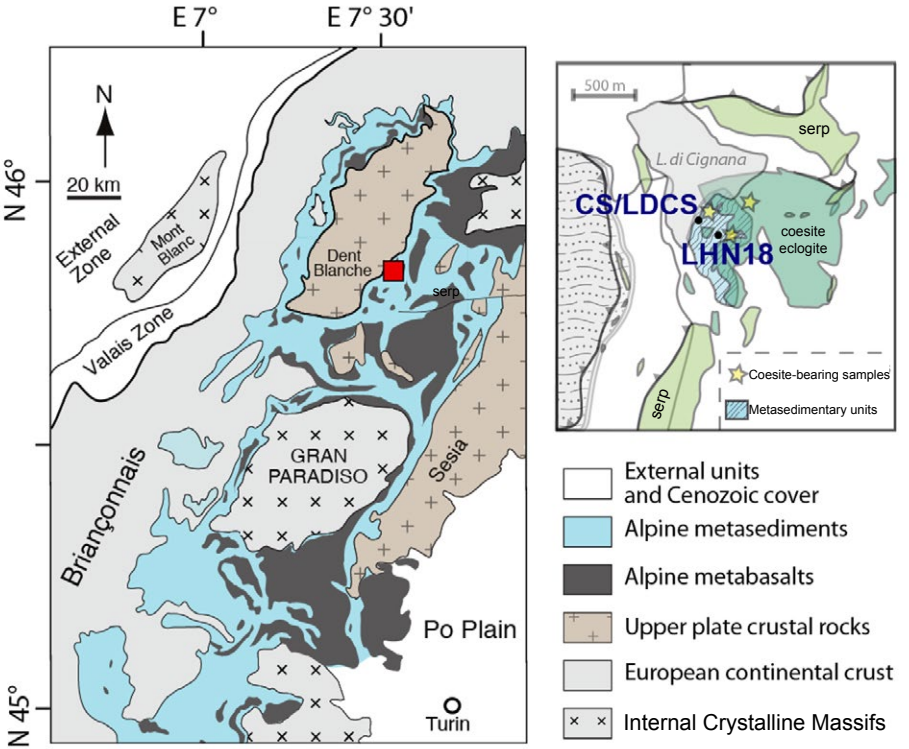

Figure 1. (A) Simplified geologic map of a part of the western Alps showing the major tectonometamorphic units and (B) map of Lago di Cignana (see the red-filled square on A) with the sampling localities for CIGSED-1 (CS), 02-LDCS-11b (LDCS), and LHN18 (small black-filled circles). The coesite-bearing samples (yellow-filled stars) indicated on the map of the Lago Cignana exposure are from van der Klauw et al. (1997). L.—Lago; serp—serpentinite.

GEOLOGIC AND PETROLOGIC FRAMEWORK

This project was founded upon the detailed framework for the metamorphic history and geochemistry of the rocks at the Lago di Cignana UHP metamorphic locality. The western Alps resulted from closure of the approximately north-south–trending Valais and Liguro-Piemontese oceans from ca. 100 Ma onward, through an east-dipping subduction zone below Apulia/Africa (see the syntheses by Angiboust et al., 2009; Agard, 2021). Metapelitic rocks and calc-schists at Cignana (field photographs in Fig. 2) were first described in detail by Reinecke (1998), who paid particular attention to phases such as garnet that preserve information regarding prograde to peak metamorphism. Garnet in these rocks, and also zircon, apatite, tourmaline, and dolomite, contains inclusions of coesite representing near-peak-pressure metamorphic conditions of the rocks, approaching 3.0 GPa (at ~575 °C; Reinecke, 1998; Angiboust et al., 2009; see also the arguments for higher peak pressure by Groppo et al., 2009; Frezzotti et al., 2011). Bebout et al. (2013) and Cook-Kollars et al. (2014) combined records from the Lago di Cignana metasedimentary rocks with those from the Schistes Lustrés exposed in the Cottian Alps, together representing

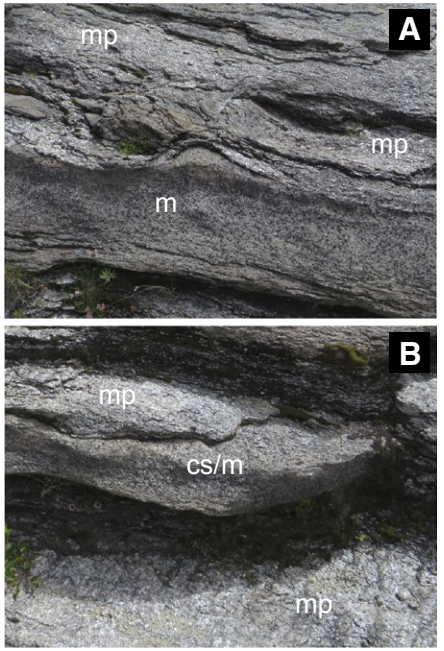

Figure 2. Field photographs of interlayered calc-schist, marble, and metapelite at the ultrahigh-pressure Lago di Cignana locality (horizontal scale is ~0.5 m; location coordinates are provided in the Supplemental Material, see text footnote 1). Abbreviations: m—marble; mp—metapelite; cs—calc-schist. The calc-schist lithology is a composition intermediate between marble and metapelite (photographs by G.E. Bebout, 2017; see the analyses of whole-rock carbonate content in Cook-Kollars et al., 2014; Epstein et al., 2020).

a subduction pressure-temperature (*P-T*) gradient of ~8 °C/km, in a detailed petrographic, petrologic, and geochemical investigation of prograde devolatilization history and element mobility. Epstein et al. (2020) conducted a regional-scale study of fluid-rock interactions and devolatilization in the Schistes Lustrés and on rocks at Lago di Cignana.

The four garnet crystals for which we present geochemical data were taken from three samples of calcite-poor metasedimentary rock collected from the same outcrops at Cignana; samples CIGSED-1 and 02-LDCS-11b came from the same metapelitic layer (see the examples of field relations in Fig. 2). Whole-rock major- and trace-element concentrations for these samples were presented by Bebout et al. (2013). Those authors also presented calculated prograde devolatilization reaction history for appropriate low-Ca metapelitic bulk compositions, based in part on investigation of the Schistes Lustrés metasedimentary complex, which provides approximate lower-grade equivalents to the rocks at Cignana (see fig. 9 in Bebout et al., 2013). The samples contain the mineral assemblage quartz + phengite + paragonite + garnet + tourmaline, with late-formed chlorite and clinozoisite (Bebout et al., 2013). The matrices of these rocks, particularly in sample LHN18B, show extensive evidence of overprinting during exhumation, as deduced by mineral assemblages and textures (Reinecke, 1998; Bebout et al., 2013). Garnet, in some cases containing coesite inclusions, preserves the most complete record of this prograde-to-peak-metamorphic element mobility (see the *P-T* path reconstructed for these rocks, largely from garnet chemistry; Reinecke, 1998). In metabasaltic rocks from the same locality, coesite occurs not only as inclusions within garnets but also as a stable phase in the matrix assemblage (showing varying degrees of conversion to quartz; see van der Klauw et al., 1997; see the photomicrograph in fig. 1 in King et al., 2004).

ANALYTICAL METHODS

We conducted high-resolution element mapping on a JEOL JXA-8530F electron probe microanalyzer (EPMA) to screen these irregularly shaped garnet crystals for best preservation of prograde growth zoning on growth-center sections. This in part involved identifying garnets in which an expected strong Y central peak and the most significant enrichment of Mn were exhibited (see the best examples in Figs. 3 and 4 for garnet crystal 02-LDCS-11b-gt3; cf. Skora et al., 2006; Moore et al., 2013). Other crystals, CIGSED1-gt1 and particularly LHN18B-gt1 (Fig. 5), were selected based on the presence of textures indicating resorption and later garnet growth. For all crystals, line traverses measured major-element composition (by EPMA), trace-element concentrations (including Li; using a Cameca 5f SIMS), and Li isotope compositions (using a Cameca 1270 SIMS). Lithium concentrations obtained by the Cameca 1270 analyses tended to be within 5% of the concentrations obtained using the Cameca 5f (despite the slightly differing locations of the "spots," which were in nearly all cases within 10 µm of the other spot). Scanning-electron microscope (SEM) methods, using a JEOL JSM-7001F, evaluated mineral inclusions and their distributions in each of these garnets. Greater detail regarding analytical methods and standardization is provided in the Supplemental Material[1]. For measurements of δ^7Li (reported relative to IAEA standard L-SVEC), uncertainty (2σ) is ~3‰.

The SIMS methodology described by Hoover et al. (2021), and employed by Penniston-Dorland et al. (2020) and Hoover et al. (2020), is broadly speaking the same as that employed in our study, resulting in similar uncertainty in the measurements. However, a notable difference is the use of glasses as standards in the other study, while our study utilized garnet working standards (previously analyzed by MC-ICP-MS) covering a wide range of major-element compositions. Both approaches were undertaken to assess and incorporate any matrix effects related to the range of garnet compositions typical in the chemically zoned garnets that were studied (see the discussion and related tables and figures in the Supplemental Material, footnote 1).

RESULTS

Figures 3–6 demonstrate key relationships among the major- and trace-element and Li concentrations and isotope compositions of the four garnet crystals for which we present data. The Supplemental Materials (footnote 1) include background element maps and EPMA line traverses for the four crystals described above. Plots of all rare earth elements (REEs) in the four crystals are also

[1]Supplemental Material. Includes the geographic coordinates for the Lago di Cignana locality, images and geochemical data for the garnets that were studied, and a description of the analytical methods. Please visit https://doi.org/10.1130/GEOS.S.19252145 to access the supplemental material, and contact editing@geosociety.org with any questions.

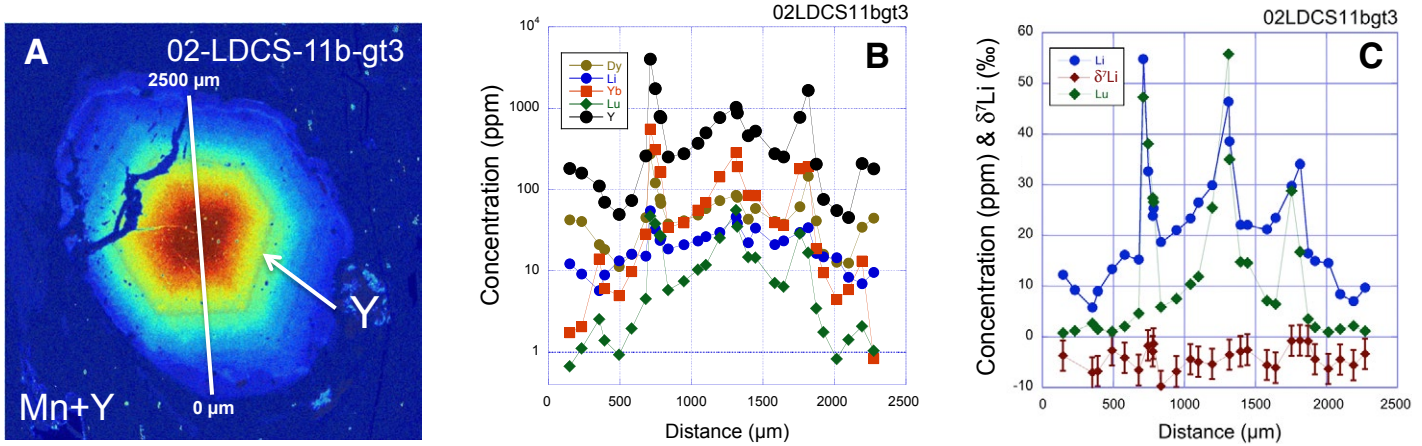

Figure 3. Compositional variation in ~2.5-mm-diameter garnet in 02-LDCS-11b-gt3. (A) Element map of Mn and Y distributions, showing concentration of Mn in the core and the position of the Y annulus (faint grayish zone at outside of yellow zone). (B) Trace-element concentrations (note the logarithmic vertical scale) across the traverse indicated in A, showing enrichments in Y, selected middle and heavy rare earth elements (MREEs and HREEs), and Li in the core and co-enrichment of these elements at the annulus (greater detail is provided in Fig. 4). (C) Lithium and Lu concentrations and δ^7Li isotope values across the same traverse, showing co-enrichments in Li and Lu and perhaps subtle increase in δ^7Li at the position of the annulus. In Figures 3, 5, and 8, δ^7Li error bars indicate 2σ of 3‰.

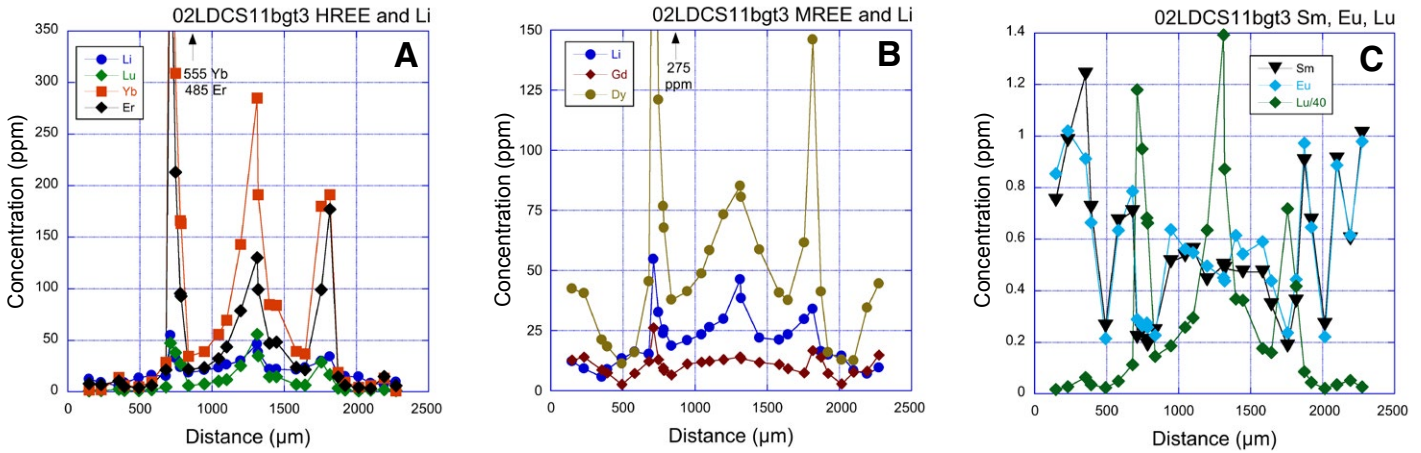

Figure 4. (A–C) Plots distinguishing the behavior of the heavy rare earth elements (HREEs) (A, B), middle rare earth elements (MREEs) (B, C), and Li in 02-LDCS-11b-gt3, the garnet best showing centering on its growth core (cf. Skora et al., 2006). Note the nonlogarithmic vertical scale to better illustrate the relationships summarized in Figure 3B. Note that each of these elements is co-enriched at the positions of the Y-rich annuli, despite the varying degrees to which they exhibit a central spike in concentration. This garnet shows only subtle variation in δ^7Li, perhaps with increase at the positions of the annulus (see Fig. 3C).

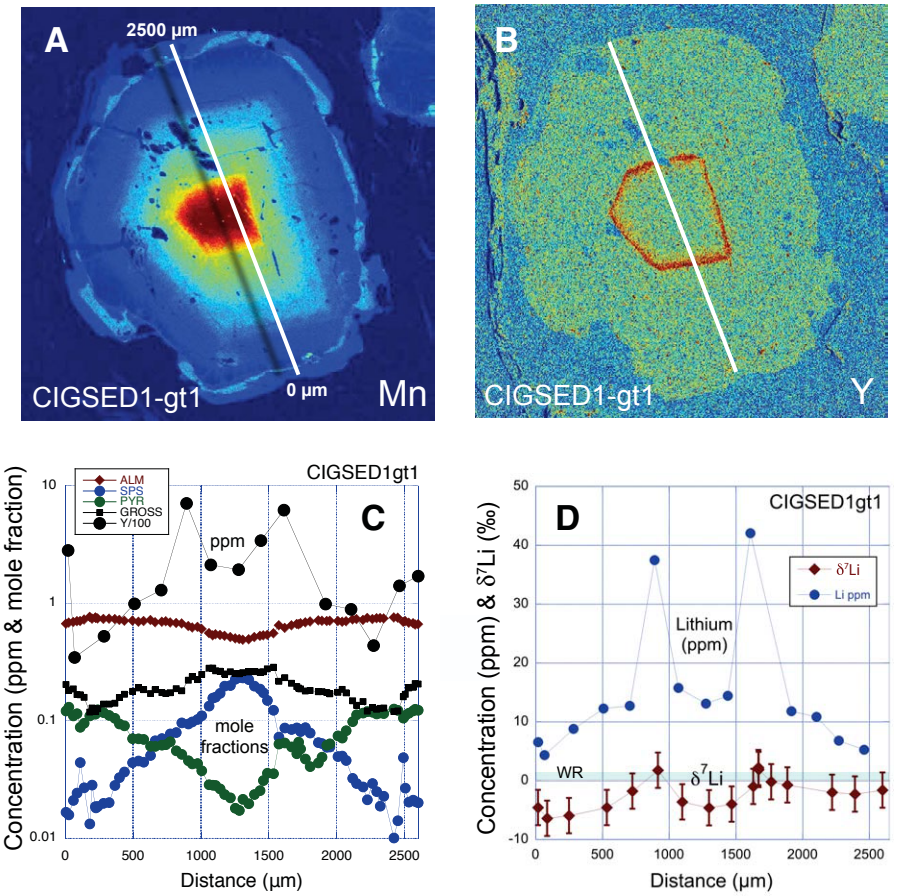

Figure 5. Compositional variation in garnet CIGSED1-gt1. (A) Mn element map, showing elevated concentration of Mn in the core. (B) Y element map, showing the position of the annulus and the slightly enriched core (slightly more yellowish in the exact core of the garnet). (C) Major-element (mole fractions of major components) and Y concentrations (ppm) across the traverse indicated in A and B, showing enrichments in Mn and Y in the core and the enrichment of Y at the position of the annulus. (D) Li concentration (ppm) and δ^7Li isotope values (‰) across the same traverse, showing enrichment in Li and apparent increase in δ^7Li at the position of the annulus. Light-blue horizontal bar represents whole-rock (WR) δ^7Li for the same rock (+0.4‰; from Barnes et al., 2019, using multicollector–inductively coupled plasma–mass spectrometry [MC-ICP-MS] methods). The similarity of the garnet δ^7Li to the whole-rock value is certainly a rough indication of the general isotopic fidelity of the secondary ion mass spectrometry calibrations and measurements. Garnet components: ALM—almandine, SPS—spessartine, PRY—pyrope, GROSS—grossular.

included as Supplemental Material, supplementing the SIMS line traverses showing REE variation.

Garnets 02-LDCS-11b-gt3, CIGSED1-gt1, and CIGSED1-gt2 showed similar chemical and isotopic features, and distributions of key mineral inclusions, but with each of these features represented to varying degrees in the individual garnets (Figs. 3–7). Garnet LHN19B-gt1 showed far more extensive resorption and later-stage garnet growth (see Fig. 8). All four of the garnet crystals were almandine-rich with strongly decreasing MnO and increasing MgO toward rims (see element maps in Figs. 3, 5, 6, and 8, core-to-rim major-element traverses in Figs. 5 and 8, and Supplemental Material, footnote 1; examples of REE-rich mineral inclusions are shown in Fig. 7). HREEs, Y, and Li also showed strong zoning, with elevated concentrations in cores (15–50 ppm Li) and marked high-concentration anomalies (up to 117 ppm Li, 5500 ppm Y, with little or no major-element shift) as growth annuli, in which some crystals had somewhat elevated δ^7Li. Figures 3 and 4 demonstrate the strong correspondence of Li enrichments in one of these crystals (02-LDCS-11b-gt3) to zones of enrichment of Y and HREEs and subtle variation in δ^7Li across the crystal. As is discussed in more detail below, the traverse of this garnet appears to have best captured the central growth core. In Figure 5, for CIGSED1-gt1, concentrations of major elements and Y are shown as a function of distance along a full-grain traverse, along with the enrichment of Li, but with a more striking elevation in δ^7Li (by ~7‰) at the position of the annulus with strong Y and HREE enrichment (see Fig. 5D).

In all crystals, rutile inclusions appeared abruptly at annuli and outward toward rims, as demonstrated in the backscattered electron (BSE) image in Figure 6B (see the element map of this garnet in Fig. 6A). In Figure 6B, the rutile grains appear as small light-gray–colored grains in the upper-right part of the image. At and outside of the annuli, concentrations of Nb in garnet were dramatically lower (see Fig. 6C). Inclusions of a highly zoned, Ca- and REE-rich phase (possibly allanite) occurred only as scattered grains outside of the annuli, toward garnet rims, and showed complex zoning in REE and Al (see examples of these grains in 02-LDCS-11b-gt3

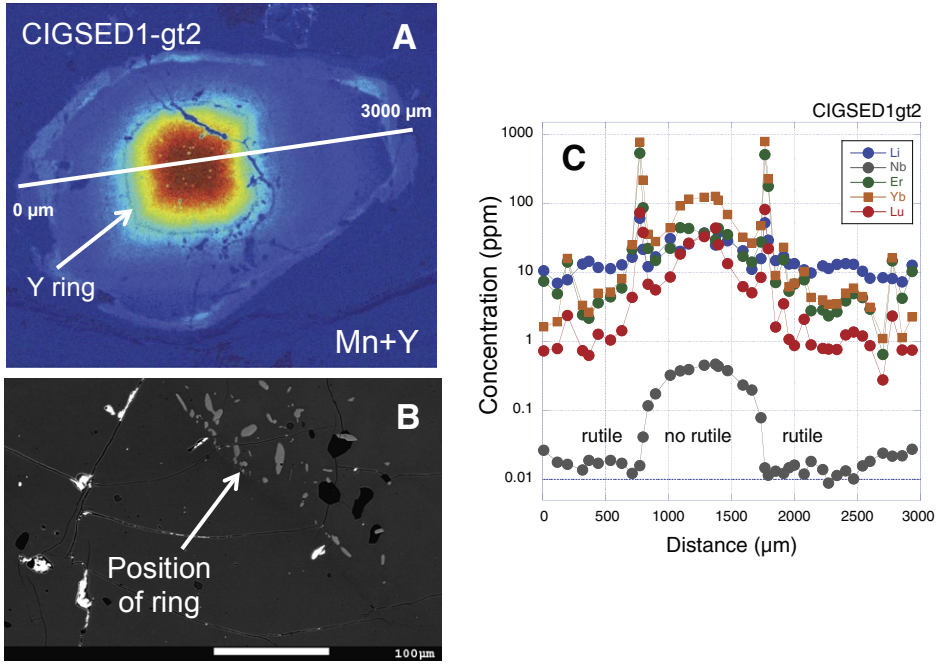

Figure 6. Compositional variation in CIGSED1-gt2. (A) Element map for Mn and Y, showing concentration of Mn in the core and the blueish Y annulus. (B) Backscattered-electron (BSE) image of an annulus region, with the core of the garnet located to the lower left. Outside of the annulus/ring, indicated by the white arrow, the garnet contains abundant inclusions of rutile (small, light-gray–colored, elongated grains). (C) Nb and heavy rare earth element (HREE) concentrations along the traverse in A. Compared with the other crystals, including gt1 in the same section, this crystal shows little compelling variation in core-to-rim δ^7Li, including relative to the annulus. Also, the central spikes in concentrations of the HREEs and Y are more muted, indicating that the traverse was somewhat offset from the growth core of the crystal (see the Supplemental Material, text footnote 1).

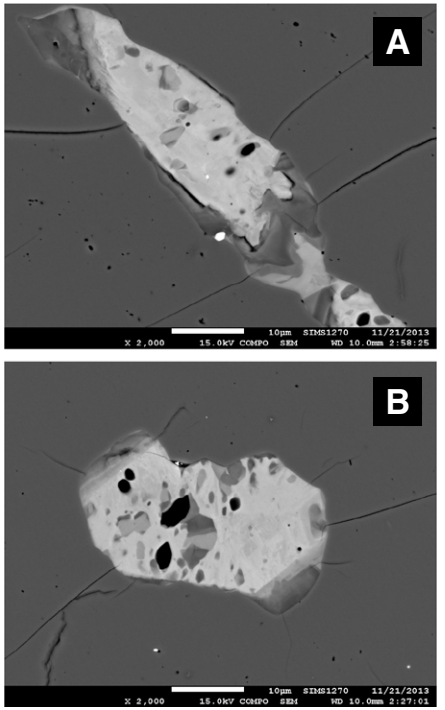

Figure 7. Examples of inclusions of a highly zoned, Ca- and rare earth element–rich phase present rimward of the annuli (backscattered-electron [BSE] images); these occur in all four of the garnets for which results are presented in this paper. Both inclusions are from 02-LDCS-11b-gt3 (see Fig. 3). These grains were confirmed as being extremely rich in light rare earth elements (LREEs) by a combination of energy-dispersive X-ray scanning electron microscope analyses and electron probe microanalysis (EPMA) element maps (lighter areas are enriched in LREEs; darker areas are enriched in Al_2O_3 and CaO).

in Fig. 7). Other mineral inclusions in garnet, based on energy-dispersive X-ray SEM imaging, included apatite, zircon, quartz, Fe-oxide, Fe-sulfide, chlorite, and phengite. Although coesite has been identified in some garnets in both metasedimentary and metabasaltic rocks at this locality (van der Klauw et al., 1997; Reinecke, 1991, 1998), the inclusions in garnet believed to be quartz showed no textural evidence of transformation from coesite to quartz and have not produced radial expansion–related fractures in the garnet.

Figure 8 presents major- and trace-element and Li isotope distributions in the garnet crystal in sample LHN18B that apparently was partially resorbed, later experiencing considerable additional growth. The region of the crystal representing this later growth contained fewer and smaller quartz inclusions than the earlier-formed garnet. The plot of major-element concentrations (Fig. 8C) demonstrates truncation of the pre-resorption zoning, in the region along the traverse at 0 to ~800 µm (left side of the diagram, upper-left part of the crystal as shown in Fig. 8A). At this same place, δ^7Li showed a strong decrease, by nearly 15‰ (Fig. 8D). The rim of the crystal adjacent to the region showing this deviation in Li isotope composition (left side in Figs. 8A and 8B) was somewhat more idioblastic than the rim around the remainder of the grain.

DISCUSSION

Origin of the Trace-Element Distributions in the Lago di Cignana Garnets

Major-element zoning in Cignana metasedimentary garnet can be viewed as reflecting prograde growth zoning, as can the strong core-to-rim depletions in HREEs and Y, on which spikes in

HREE, Y, and Li concentrations are superimposed in response to reaction history. The garnet crystals grew in a matrix containing Li-rich phengite (current phengite Li abundances are ~99 ppm in CIGSED-1 and ~37 ppm in LHN18B; SIMS data by Bebout et al., 2013) and, at earlier stages, chlorite (see the prograde reaction history calculated by Bebout et al., 2013). Uptake of Li, however, predominantly reflects co-enrichment along with Y + REEs, due to mutual incorporation via a charge-coupled substitution, where the [$YLiM_{-2}$] exchange vector is the most energetically favorable means of Li incorporation in garnet (see Carlson et al., 2014). Thus, increased Li uptake is a passive consequence of elevated concentrations of Y + REEs. Correlations in the enrichments of Y, HREEs, and Li are particularly strong at/near the annuli.

In metamorphic garnet, gradients in the concentrations of Y and REEs can in some cases reflect diffusion-limited uptake during crystal growth, as a consequence of differing intergranular diffusion rates for these trace elements (Skora et al., 2006; Moore et al., 2013). Skora et al. (2006) documented examples in which Y and REEs arrived sequentially to a growing garnet crystal, as a function of change in REE intergranular diffusion rates with increasing temperature during depletion of these elements in the matrix. Central peaks in garnet crystals experiencing this process become higher and sharper with increasing atomic number, suggesting growth with uptake from the matrix of elements governed by differing rates of incorporation of ions onto garnet surfaces. The trace-element distributions in the Cignana garnets that we describe here to some degree exhibit the core/near-core trace-element patterns outlined by Skora et al. (2006) and attributed by those authors to diffusion-limited uptake. In the Cignana garnets, Y, the HREEs (Yb, Lu, and Er), and Li showed strong central spikes in concentration in the best-centered traverse (02-LDCS-11b-gt3; see Figs. 3B, 3C, and 4A). Middle rare earth element (MREE) Dy similarly showed a pronounced central spike, although less sharp than for Lu, Yb, and Er (Figs. 3B and 4B), rather than the concave-up pattern in garnet cores reported by Skora et al. (2006). Another MREE, Gd, showed only a subtle convex-up pattern

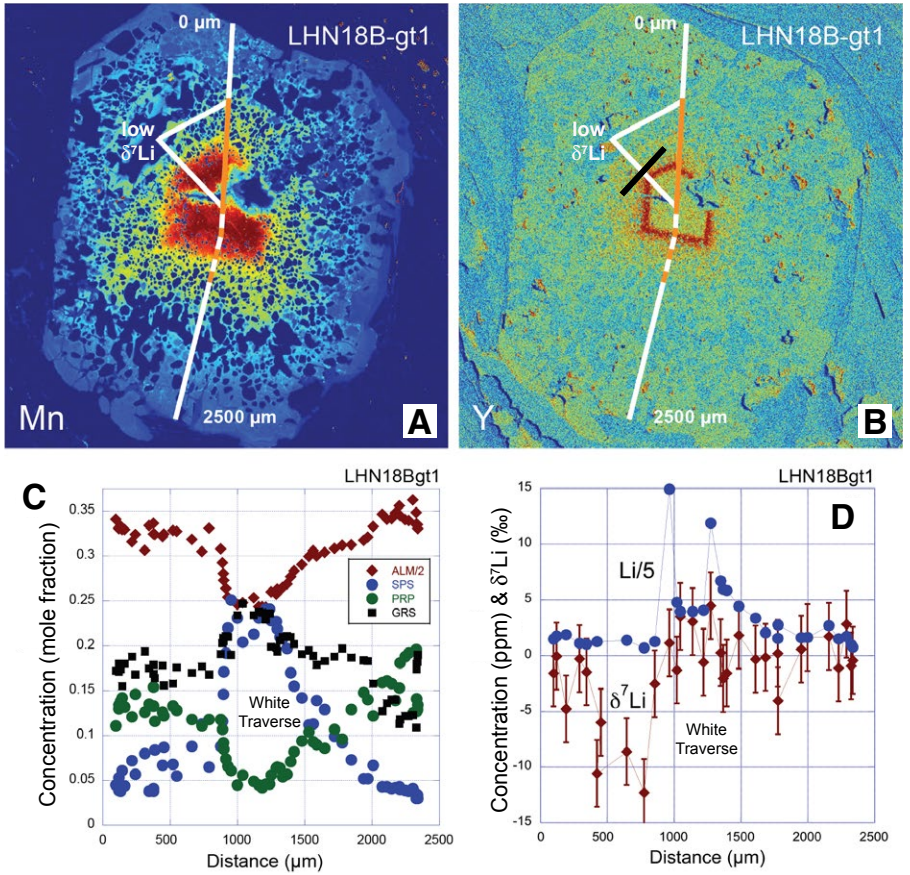

Figure 8. Compositional variation in garnet LHN18B-gt1. (A) Mn element map showing high concentration of Mn in/near the growth core. (B) Y concentration map showing the position of the annulus. (C) Major-element composition along the traverse in A and B. (D) Lithium concentration (ppm) and δ^7Li isotope value (‰) along the traverse indicated in A and B; this initial traverse (white line) was selected to avoid areas with particularly high densities of mineral inclusions. A later traverse (orange line) that partly overlapped this earlier traverse avoided this low-δ^7Li region and produced an element/isotope pattern similar to that in Figures 3–6 (also see the Supplemental Material, text footnote 1). Dashed orange and white segment of the line indicates overlap by the two traverses, and black line in B indicates the position in the garnet where the transition in δ^7Li and major-element composition is observed (see the labeling of the low-δ^7Li region). Garnet components: ALM—almandine, SPS—spessartine, PRP—pyrope, GRS—grossular.

("hump") in the garnet core region (Fig. 4B). The lower-atomic-number Sm and Eu occurred at very low concentrations (0.2–1.25 ppm), showing a faint convex-up pattern in the core, possible minor depletion at the location of the Y-rich annulus, perhaps related to uptake of light rare earth elements (LREEs) by the allanite-like phase stabilized at/outside the annuli (see Fig. 7), and minor enrichments toward the rims, perhaps similar to those reported by Skora et al. (2006) (see Fig. 4C). LREE

concentrations showed no convincing trends along the same traverse and were low, near 0.1 ppm for Nd, near 0.01 ppm for Ce, and near 0.005 ppm for La and Pr. The HREEs and MREEs Dy and Gd, and Li showed strong enrichment in the same locations outward from the cores, at the position of the Y-rich annuli, as shown in all traverses (see Figs. 3–6 and 8). These strong enrichments at the annuli could have complicated the development of, or obscured, any strong rimward peaks (the "second maxima" of Skora et al., 2006; see fig. 3 in that paper) for Y and the REEs Er, Dy, and Gd (or the enrichments closer to rims for Sm and Eu noted by those authors).

Although the three garnet crystals for which compositions are shown in Figures 3–6 all displayed an annulus with strong co-enrichments, the traverse of crystal 02-LDCS-11b-gt3 (Fig. 3) showed the most-pronounced "spike" in concentrations of the elements expected in the immediate core growth position (cf. Skora et al., 2006; Moore et al., 2013). The sectioning of crystal CIGSED1-gt1 (Fig. 5) apparently missed the very small growth center that contains this spike, and the sectioning of crystal CIGSED1-gt2 (Fig. 6) was apparently very slightly offset from the growth center, showing less pronounced enrichment in HREEs, Y, and Li in cores (Fig. 6C; also see the Supplemental Material, footnote 1).

Prograde garnet-forming reaction(s) in these rocks in part involved titanite breakdown to stabilize rutile, resulting in delivery of more abundant Y and HREEs at surfaces of growing garnets to produce the prominent annuli observed in all crystals examined in this study. However, no titanite was identified as inclusions in the garnets inside the annuli. King et al. (2004), in studies of metabasaltic garnets at the Cignana locality, attributed similar anomalies in Y + HREE to the breakdown of titanite via the following reaction, which could also explain the relationships presented in this paper (perhaps involving lawsonite rather than clinozoisite):

$$2\ \text{clinozoisite} + 5\ \text{titanite} = 3\ \text{grossular} + 5\ \text{rutile} + 2\ \text{quartz/coesite} + H_2O. \quad (1)$$

Mechanisms for Delivery of Isotopically Fractionated Lithium to UHP Garnets

The distributions of $\delta^7Li_{L\text{-}SVEC}$ in these garnet crystals are complex, in some cases showing only subtle core-to-rim variation other than at Y + REE annuli. At annuli, some crystals display elevated δ^7Li (by up to 7‰; Fig. 5), whereas others do not, at least not as obviously (see Figs. 3 and 4). One possible scenario for the production of such an isotope effect is that Li isotopes could have been more fractionated by diffusive delivery to some growing garnet crystals before and after growth at annuli, where the garnet δ^7Li values in the annuli are similar those of the whole rock (+0.4‰; see Fig. 5D; Barnes et al., 2019). During prograde garnet growth and uptake of Li, before and after production of the annuli (as related to uptake of Y and HREEs), ^{6}Li could have diffused more rapidly than ^{7}Li to the garnet interface, resulting in lowered δ^7Li (relative to that equilibrated with the matrix assemblage). More rapid advective delivery of Li to the growing garnet to produce the annuli could have provided less-fractionated Li and higher δ^7Li near that of the whole rock. This more advective delivery of Li could have resulted from the reaction involving breakdown of titanite to produce rutile (see the example reaction in Eq. 1 above), producing a pulse in the production of fluid (cf. Tan et al., 2020). More rigorous consideration of these conceptual models is limited by the unknown extent of intermineral isotope fractionation (garnet versus minerals in the whole-rock assemblage, in particular, chlorite, phengite, and paragonite; see the SIMS data for these phases in Bebout et al., 2013) and the effect of a changing matrix mineral assemblage on the δ^7Li values of a growing garnet crystal (see the thermodynamic calculations of prograde mineral reactions in Bebout et al., 2013). Penniston-Dorland et al. (2017) provided a compilation of fluid-mineral Li isotope fractionation factors, including those for various phyllosilicates (e.g., smectite, illite, muscovite); however, various garnet-mineral fractionation factors are still lacking. The isotope shifts that are possible, due to equilibrium isotope fractionation during processes such as devolatilization, are regarded as being rather small, perhaps only a few per mil. Thus, the wide range of δ^7Li in rocks and minerals could in part reflect kinetic isotopic fractionation (see Penniston-Dorland et al., 2017, 2020).

For garnet LHN18B-gt1, the large change in Li concentration and isotopic composition (downward shift in δ^7Li), correlated with major/trace-element variation, could reflect a change in the mechanism of delivery of Li to the garnet interfaces (cf. Moore et al., 2013). The resorption observed for this garnet (Fig. 8) likely occurred during the early exhumation history of the rocks, at *P-T* conditions that stabilized coarse-grained paragonite-bearing mineral assemblages overgrowing the dominant foliation of the rocks (see the discussion by Reinecke, 1998; cf. Bebout et al., 2013). Although these low δ^7Li values could directly reflect the δ^7Li of an infiltrating fluid from an external source, a suitably low-δ^7Li source for this fluid is not apparent, and it is quite likely that the low-δ^7Li signature reflects kinetic fractionation during diffusive delivery, in pore fluid, toward the growing garnet, as described for growth of the other garnets studied here, aside from at annuli (cf. Hoover et al., 2020; discussion by Penniston-Dorland et al., 2020). The latter explanation is perhaps more likely to have produced the extremely low δ^7Li values observed in parts of this garnet (near –12‰). Exhumation-related overprinting, perhaps related to open-system fluid infiltration, has been invoked for production of the overgrowths on Cignana metasedimentary tourmaline with distinct mineral inclusions, lowered Mg/Fe^{+2}, and elevated δ^{11}B described by Bebout and Nakamura (2003). These authors did not explore the possibility that the observed shifts in tourmaline δ^{11}B (by up to 15‰) could reflect a kinetic fractionation associated with differing intergranular diffusivities of the two B isotopes.

Significance for Ocean-Mantle Lithium Transfer along the Subduction Pathway

The results of this study, integrated with those of Bebout et al. (2013) and Barnes et al. (2019), indicate impressive retention of Li in deeply subducted pelitic rocks, to depths approaching those beneath volcanic fronts, despite redistribution

during complex devolatilization reaction histories. These studies documented only subtle hints of decreased Li concentrations with increasing metamorphic grade along the ~8 °C/km geotherm thought to reflect western Alps paleo–subduction zone conditions. Bebout et al. (2013) demonstrated that, with the breakdown of Li-rich chlorite, Li was increasingly transferred into phengite, resulting in an increase in Li concentrations in phengite at the higher grades (see fig. 11 in that paper). Except at the annuli, where concentrations in some cases exceed 100 ppm, the Li concentrations of garnets in the Cignana metapelites were relatively low (range of ~10–30 ppm). Because of this, and the relatively small modal abundance of garnet, the incorporation of Li into garnet did not produce a noticeable reduction in Li concentration in the phengite in the matrix. Barnes et al. (2019) suggested that an increase in δ^7Li with increasing grade in the western Alps metasedimentary suite can be related to the chemical index of alteration of the protoliths of the rocks and is not likely to reflect isotopic fractionation during loss of Li to fluids during devolatilization reactions (also see the discussion by Penniston-Dorland et al., 2011).

CONCLUSIONS

Our results constitute an initial description of correlated core-to-rim variations in concentrations of major elements, Li, HREEs, and Y, and δ^7Li values in relatively high-Li UHP metasedimentary garnets. They demonstrate the potential utility of Li concentrations and isotope compositions in garnet for elucidating reaction history in rocks for which the peak-metamorphic matrix mineral assemblages have been extensively overprinted during exhumation (for a description of metabasaltic garnets at this locality, also see King et al., 2004). A tantalizing possibility raised by these observations (and in other recent studies) is that differing intergranular diffusion rates of ^{7}Li and ^{6}Li could produce significant Li isotope fractionation at the surface of a growing garnet crystal. Small-scale fluctuations in δ^7Li observed in some garnets correlate with abrupt shifts in major- and trace-element concentrations, suggesting that changes in reactant phases exerted some control on the evolution of δ^7Li. In some cases, large changes in Li concentration and isotopic composition, correlated with major/trace-element variation, could represent open-system behavior involving transport of Li in infiltrating fluids, with or without diffusive effects governing the δ^7Li value upon arrival at garnet growth interfaces (this study; Penniston-Dorland et al., 2020; Hoover et al., 2020).

ACKNOWLEDGMENTS

This research was funded largely by grants from the 21st Century Center of Excellence Program, Japanese Ministry of Education, Science, Sports, and Culture (to E. Nakamura), with some support also from National Science Foundation grants EAR-0079331 and EAR-0711355 (to G.E. Bebout). We thank Sarah Penniston-Dorland and Besim Dragovic for reviews of an earlier version of this manuscript, and Besim Dragovic and an anonymous reviewer for their comments on this manuscript for *Geosphere*. Finally, we thank Tatsuki Tsujimori and Yuri Shimaki for their assistance in the earlier stages of data acquisition at the Pheasant Memorial Laboratory for Geochemistry and Cosmochemistry.

REFERENCES CITED

Agard, P., 2021, Subduction of oceanic lithosphere in the Alps: Selective and archetypal from (slow-spreading) oceans: Earth-Science Reviews, v. 214, https://doi.org/10.1016/j.earscirev.2021.103517.

Angiboust, S., Agard, P., Jolivet, L., and Beyssac, O., 2009, The Zermatt–Saas ophiolite: The largest (60-km wide) and deepest (c. 70–80 km) continuous slice of oceanic lithosphere detached from a subduction zone?: Terra Nova, v. 21, p. 171–180, https://doi.org/10.1111/j.1365-3121.2009.00870.x.

Barnes, J.M., Penniston-Dorland, S.C., Bebout, G.E., Hoover, W., Beaudoin, G.M., Selverstone, J., and Agard, P., 2019, Chlorine and lithium behavior in metasedimentary rocks during prograde metamorphism: A comparative study of exhumed subduction complexes (Catalina Schist and Schistes Lustrés): Chemical Geology, v. 336–337, p. 40–53, https://doi.org/10.1016/j.lithos.2019.03.028.

Bebout, G.E., and Nakamura, E., 2003, Record in metamorphic tourmalines of subduction-zone devolatilization and boron cycling: Geology, v. 31, p. 407–410, https://doi.org/10.1130/0091-7613(2003)031<0407:RIMTOS>2.0.CO;2.

Bebout, G.E., Agard, P., Kobayashi, K., Moriguti, T., and Nakamura, E., 2013, Devolatilization history and trace element mobility in deeply subducted sedimentary rocks: SIMS evidence from western Alps HP/UHP suites: Chemical Geology, v. 342, p. 1–20, https://doi.org/10.1016/j.chemgeo.2013.01.009.

Cahalan, R.C., Kelly, E.D., and Carlson, W.D., 2014, Rates of Li diffusion in garnet: Coupled transport of Li and Y + REEs: The American Mineralogist, v. 99, p. 1676–1682, https://doi.org/10.2138/am.2014.4676.

Carlson, W.D., Gale, J.D., and Wright, K., 2014, Incorporation of Y and REEs in aluminosilicate garnet: Energetics from atomistic simulation: The American Mineralogist, v. 99, p. 1022–1034, https://doi.org/10.2138/am.2014.4720.

Cook-Kollars, J.E., Bebout, G.E., Collins, N., Angiboust, S., and Agard, P., 2014, Subduction-zone metamorphic pathway for deep carbon cycling: Evidence from HP/UHP metasedimentary rocks, Italian Alps: Chemical Geology, v. 386, p. 31–48, https://doi.org/10.1016/j.chemgeo.2014.07.013.

Epstein, G.S., Bebout, G.E., Angiboust, S., and Agard, P., 2020, Scales of fluid-rock interaction and carbon mobility in the deeply underplated and HP-metamorphosed Schistes Lustrés, western Alps: Lithos, v. 354–355, https://doi.org/10.1016/j.lithos.2019.105229.

Frezzotti, M.L., Selverstone, J., Sharp, Z.D., and Compagnoni, R., 2011, Carbonate dissolution during subduction revealed by diamond-bearing rocks from the Alps: Nature Geoscience, v. 4, p. 703–706, https://doi.org/10.1038/ngeo1246.

Groppo, C., Beltrando, M., and Compagnoni, R., 2009, The *P-T* path of the ultra-high pressure Lago di Cignana and adjoining high-pressure meta-ophiolitic units: Insights into the evolution of the subducting Tethyan slab: Journal of Metamorphic Geology, v. 27, p. 207–231, https://doi.org/10.1111/j.1525-1314.2009.00814.x.

Hoover, W.F., Penniston-Dorland, S., Baumgartner, L.P., Bouvier, A.S., and Dragovic, B., 2020, Cyclic fluid flow in a high-pressure shear zone: Insights from Li isotope zoning in garnet: Abstract V051–05 presented at 2020 Fall Meeting, AGU, online, 1–17 December.

Hoover, W.F., Penniston-Dorland, S.C., Baumgartner, L.P., Bouvier, A.-S., Baker, D., Dragovic, B., and Gion, A., 2021, A method for secondary ion mass spectrometry measurement of lithium isotopes in garnet: The utility of glass reference materials: Geostandards and Geoanalytical Research, v. 45, no. 3, p. 477–499, https://doi.org/10.1111/ggr.12383.

John, T., Gussone, N., Podladchikov, Y.Y., Bebout, G.E., Dohmen, R., Halama, R., Klemd, R., Magna, T., and Seitz, M., 2012, Pulsed long-distance fluid flow through subducting slabs feeds volcanic arcs: Nature Geoscience, v. 5, p. 489–492, https://doi.org/10.1038/ngeo1482.

King, R.L., Bebout, G.E., Kobayashi, K., Nakamura, E., and van der Klauw, S.N.G.C., 2004, Ultrahigh-pressure metabasaltic garnets as probes into deep subduction zone chemical cycling: Geochemistry Geophysics Geosystems, v. 5, Q12J14, https://doi.org/10.1029/2004GC000746.

Moore, S.J., Carlson, W.D., and Hesse, M.A., 2013, Origins of yttrium and rare earth element distributions in metamorphic garnet: Journal of Metamorphic Geology, v. 31, p. 663–689, https://doi.org/10.1111/jmg.12039.

Penniston-Dorland, S., Liu, X.-M., and Rudnick, R.L., 2017, Lithium isotope geochemistry: Reviews in Mineralogy and Geochemistry, v. 82, p. 165–217, https://doi.org/10.2138/rmg.2017.82.6.

Penniston-Dorland, S.C., Bebout, G.E., Pogge von Strandmann, A.E., Elliott, T., and Sorensen, S.S., 2011, Lithium and its isotopes as tracers of forearc fluids and metasomatic processes: Evidence from the Catalina Schist, California, USA: Geochimica et Cosmochimica Acta, v. 77, p. 530–545, https://doi.org/10.1016/j.gca.2011.10.038.

Penniston-Dorland, S.C., Baumgartner, L.P., Dragovic, B., and Bouvier, A.-S., 2020, Li isotope zoning in garnet from

Franciscan eclogite and amphibolite: The role of subduction-related fluids: Geochimica et Cosmochimica Acta, v. 286, p. 198–213, https://doi.org/10.1016/j.gca.2020.07.025.
Reinecke, T., 1991, Very-high-pressure metamorphism and uplift of coesite-bearing metasediments from the Zermatt-Saas zone, western Alps: European Journal of Mineralogy, v. 3, no. 1, p. 7–18, https://doi.org/10.1127/ejm/3/1/0007.
Reinecke, T., 1998, Prograde high- to ultrahigh-pressure metamorphism and exhumation of oceanic sediments at Lago di Cignana, Zermatt–Saas zone, western Alps: Lithos, v. 42, p. 147–189, https://doi.org/10.1016/S0024-4937(97)00041-8.
Skora, S., Baumgartner, L.P., Mahlen, N.J., Johnson, C.M., Pilet, S., and Hellebrand, E., 2006, Diffusion-limited REE uptake by eclogite garnets and its consequences for Lu-Hf and Sm-Nd geochronology: Contributions to Mineralogy and Petrology, v. 152, p. 703–720, https://doi.org/10.1007/s00410-006-0128-x.
Tan, Z., Agard, P., Gao, J., Hong, T., and Wan, B., 2020, Concordant pulse in Mn, Y and HREEs concentrations during UHP eclogitic garnet growth: Transient rock dynamics along a cold subduction plate interface: Earth and Planetary Science Letters, v. 530, https://doi.org/10.1016/j.epsl.2019.115908.
van der Klauw, S.N.G.C., Reinecke, T., and Stockhert, B., 1997, Exhumation of ultrahigh-pressure metamorphic oceanic crust from Lago di Cignana, Piemontese zone, western Alps: The structural record in metabasites: Lithos, v. 41, p. 79–102, https://doi.org/10.1016/S0024-4937(97)82006-3.